Rapid Communication

Size and temperature effects on dielectric breakdown of ferroelectric films

Sheng TONG*

DePaul University, 1 E. Jackson Blvd., Chicago, IL 60604, USA

Abstract: The paper introduces a model of dielectric breakdown strength. The model integrated thermal breakdown and defect models, representing the relationship between the electric field of ferroelectric films and dimensional parameters and operating temperature. This model is verified with experimental results of the lead lanthanum zirconate titanate (PLZT) films of various film thickness ($d = 0.8$–3 μm), electrode area ($A = 0.0020$–25 mm^2) tested under a range of operating temperature ($T = 300$–400 K) with satisfying fitting results. Also learned is a relationship that the recoverable electric energy density is directly proportional to the square of breakdown electric field. This relationship is found viable in predicting the electric energy density in terms of variables of d, A, and T for the PLZT films.

Keywords: film thickness; electrode size; ceramics; energy storage

There has been a great interest in the dielectric breakdown (DBD) of the ferroelectric films for their important applications in passive devices, field emission transistors, and ferroelectric random-access memory (FeRAM). In these devices, DBD strength determines the degree of the integration and the magnitude of energy loss [1–3]. In particular, high performance energy storage capacitors require large DBD electric field (E_b) and relative permittivity (ε_r). The recoverable electric energy density (U_{reco}) is calculated using the following equation [4]:

$$U_{reco} = \int_{E_b}^{0} \varepsilon_0 \varepsilon_r E \mathrm{d}E \tag{1}$$

where ε_0 is the permittivity of vacuum. Early works on the mechanisms of DBD in high permittivity dielectrics (like ferroelectrics) found that the failure was not intrinsic in nature. That is, electronic breakdown featuring bond breaking and oxygen removal was not observed [5–8]. In this fashion, thermal breakdowns (TBD), such as dc TBD, impulse TBD, and avalanche breakdown, always dominate prior to intrinsic DBD. High-permittivity ferroelectric materials are characterized by their wide band-gap and electrical-to-thermal conductivity ratio (σ/κ). Therefore, TBD is a commonly observed behavior in these materials including semiconductors and insulators [6]. Key factors dominating the breakdown strength of ferroelectric devices extrinsically include dielectric/electrode material properties (composition, microstructure), device structure (size, shape), and operational conditions (voltage ramp rate, temperature) [5,6,9–17]. There have been extensive research on the individual effect of dielectric thickness (d), electrode area (A), and temperature (T) on the breakdown strength of typical ferroelectric materials such as Pb(Zr,Ti)O$_3$, (Pb,La)(Zr,Ti)O$_3$(PLZT), BaTiO$_3$, (Ba,Sr)TiO$_3$, etc. [5,6,9–12,14–16]. However, a unified model on these

* Corresponding author.
E-mail: shengtg@gmail.com

parameters that affect DBD is yet to be developed. In this work, a model is developed on the correlation between E_b and other key material factors, such as dielectric thickness, area, and temperature. The validity of the model was tested by measurements of E_b of PLZT films.

Previous research suggested the dc TBD is the main mechanism, responsible for failure in high-ε_r dielectrics [5,6,16], although defect density was not considered. In these models, the dc electric field ramp rate is $\gg 1$ μs and the relationship between T and E_b is as follows [6,15].

$$-\kappa\nabla^2 T = \sigma E_b^2 \qquad (2)$$

It has also been reported that E_b is inversely proportional to thickness (d) which is mainly determined by the thermal distribution across the dielectric thickness and the bulk/surface thermal conductivity of the material [17–19]. Below a critical dielectric thickness, a power relationship between dielectric strength field (E_b) and d has been established [5,9,11]:

$$E_b = cd^{-\alpha} \exp(E_a/2kT) \qquad (3)$$

where c is a constant, E_a is the activation energy, and k is the Boltzmann constant. The exponent α has a theoretical value of 0.5 [11,17,18] while experimental values have been observed to vary between 0 and 1 depending on the processing conditions, thickness, etc. [5,7,9].

Although the TBD model in Eq. (3) provides the relationship between d and E_b of the ferroelectric films at large, the electrode area is not included. According to the thermal models [5,6,16,19], heat generated during TBD can be effectively removed from the surface area of the dielectric, leading to an increase in E_b. This is in contrast to the experimentally observed decrease in E_b with increasing electrode area. However, this discrepancy can be explained by considering the probability of finding a more defective column with increase in area [12]. In practice, due to the defective nature of the capacitors, a number of samples are measured to statistically determine the reliable E_b values. For example, one widely adopted method to determine average E_b (E_A) is the Weibull distribution [20].

Defect models based on probability start with a small volume of defect randomly distributed in the bulk of the material. If the ferroelectric thin film is divided into a large number of small cubes with an edge length of a representing the smallest defect size, the column (consisting of a stack of the cubes vertical to the surface)

with the most defects can form a conducting path for the breakdown (Fig. 1(a)). This model is known as the weakest phase breakdown model [5,12,21,22]. In the case of a larger electrode area, the probability of finding a conductive path under the electrode increases, leading to a reduction in E_b. As mentioned previously, the typical defective failure analysis is usually based on testing samples by varying several parameters (T, d, and A) while keeping one of which a constant. In Weibull analysis, the cumulative probability (F) corresponding to E_b is expressed as follows [20]:

$$F(A) = 1 - e^{-\left(\frac{E_b}{E_A}\right)^n} \qquad (4)$$

where F is the sample cumulative distributive parameter and n is the fitting parameter. E_b is equal to E_A when $F = 1 - 1/e$. That is, at least one of such most defected unit columns is included under the electrode of area A. If a series of unit columns ($A_0 = a^2$) are tested, the values of F as a function of E_b can be illustrated as shown in Fig. 1(b). When a series of electrode area of A_1 capacitors is tested, each column contains number of (A_1/A_0) unit columns. Thus, to ensure E_b to be greater than or equal to a certain value, each column must have less or equal number of defects defined by the value of
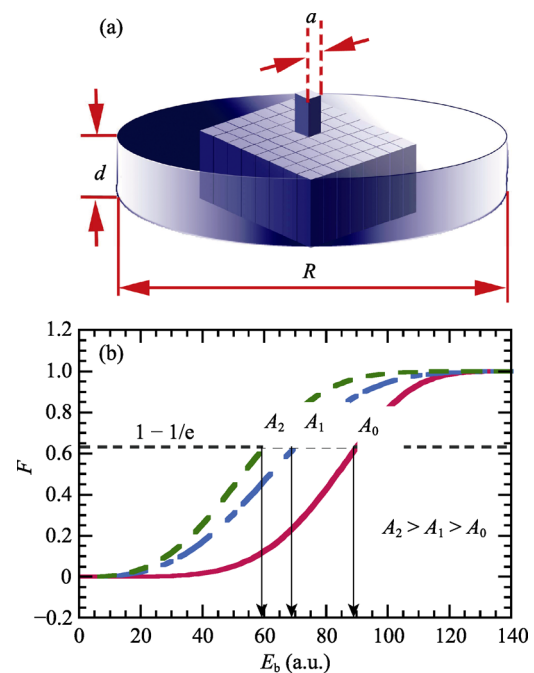
Fig. 1 (a) Illustration of a ferroelectric film with a thickness (d) and diameter (R) divided into small square columns with an edge length of a for defect dielectric breakdown model analysis. (b) Weibull cumulative distribution function of the effect of electrode area on the average dielectric breakdown electric field (E_A).

E_b. That is, the relationship between the cumulative probability of E_b for the electrode area of A_1 and that for the electrode area of A_0 can be expressed as follows:

$$1 - F(A_1) = [1 - F(A_0)]^{\frac{A_1}{A_0}} \tag{5}$$

Using Eq. (4) and Eq. (5), we get

$$E_{A_1} = E_{A_0} \left(\frac{A_1}{A_0} \right)^{-n^{-1}} \tag{6}$$

E_A of a finite electrode area is smaller than that of a unit column since n is typically greater than that of an increasing failure rate [23]. As shown in Fig. 1(b), the electrode area of A_1 greater than unit column leads to $E_{A_1} < E_{A_0}$, and a larger electrode area $A_2 > A_1$ can result in a further reduced E_A. Assuming the BD strength of a unit column E_{A_0} follows Eq. (2), it can be deduced that

$$E_A = cd^{-\alpha} A^{-n} \exp(E_a / 2kT) \tag{7}$$

where c, α, k are the fitting parameters, E_a is the activation energy, and k is the Boltzmann constant. Equation (7) describes the interdependence of three variables, d, A, and T, that determine E_A of the ferroelectric films. For any of the two variables being constant, the equation is reduced to Eqs. (3) and (6), which has been widely discussed [5,9,11,15].

To validate Eq. (7), the lead lanthanum zirconate titanate (Pb$_{0.92}$La$_{0.08}$Zr$_{0.52}$Ti$_{0.48}$O$_3$, PLZT) films were deposited on the lanthanum nickel oxide buffered

nickel substrates using chemical solution deposition with different thicknesses ($d \approx 0.8$, 1.0, 1.3, 1.6, 2.0, 3.0 μm) and electrode sizes ($A \approx 0.0020$, 0.0078, 0.0491, 0.441, 25 mm^2), and measured the E_b under different temperatures ($T \approx 300$, 325, 350, 375, 400 K). The fabrication and measurements of PLZT films were reported previously [4]. For each condition, E_b was measured on thirty samples for use in the Weibull analysis. Figures 2(a)–2(c) show the Weibull statistical distribution of E_b for various film thicknesses, electrode areas, and measurement temperatures. The experimental curves are fitted using Eqs. (4) and (8) [24]:

$$F = (i - 0.3) / (n + 0.4) \tag{8}$$

where i is the sample sequence number and n is the total number of sample ($n = 30$). It can be seen in Figs. 2(a)–2(c), within the experiments conducted, electrode area exhibits the strongest effect on E_b, whereas E_b is almost independent of temperature between 300 and 400 K. The calculated E_A from Fig. 2(a)–2(c) is plotted in Figs. 3(a)–3(c) as a function of d, A, and T, with the error bars representing the measured E_b range.

The effects of thickness, area, and temperature on E_A are fitted using individual models based on Eqs. (3) and (6) and represented as solid red lines in Figs. 3(a)–3(c). As can be seen in the figure, the individual equations effectively describe the dependence of E_A on all three individual parameters with correlation coefficients between 0.88 and 0.99. It is observed that the E_A of PLZT films follows the TBD model based on d and T similar to that observed by others [10,11,13]. The
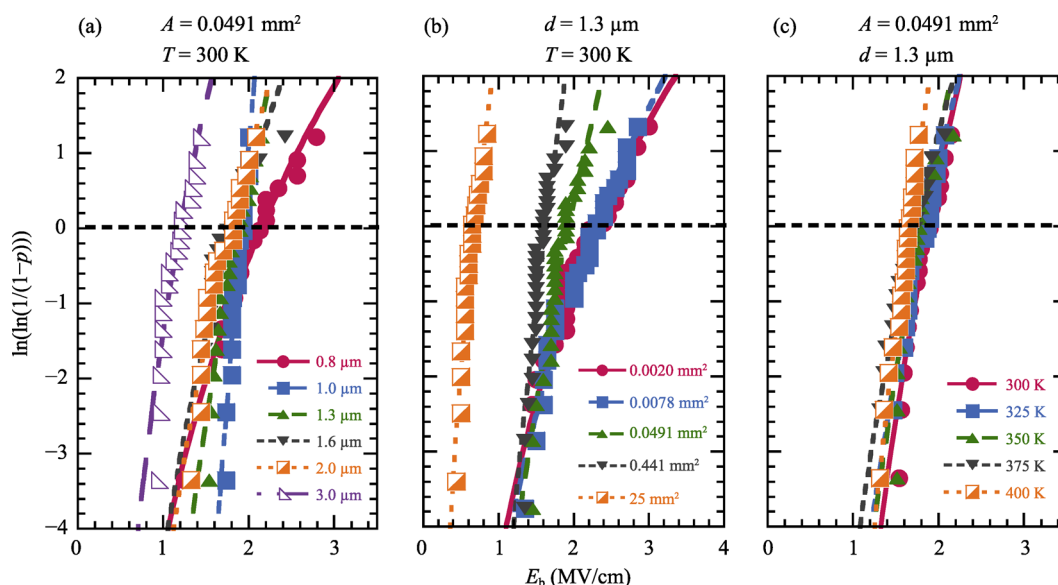
Fig. 2 Weibull failure estimation of dielectric breakdown electric field (E_b) of PLZT films in different film thickness (a), electrode area (b), and under various temperature (c) ($R > 0.987$).
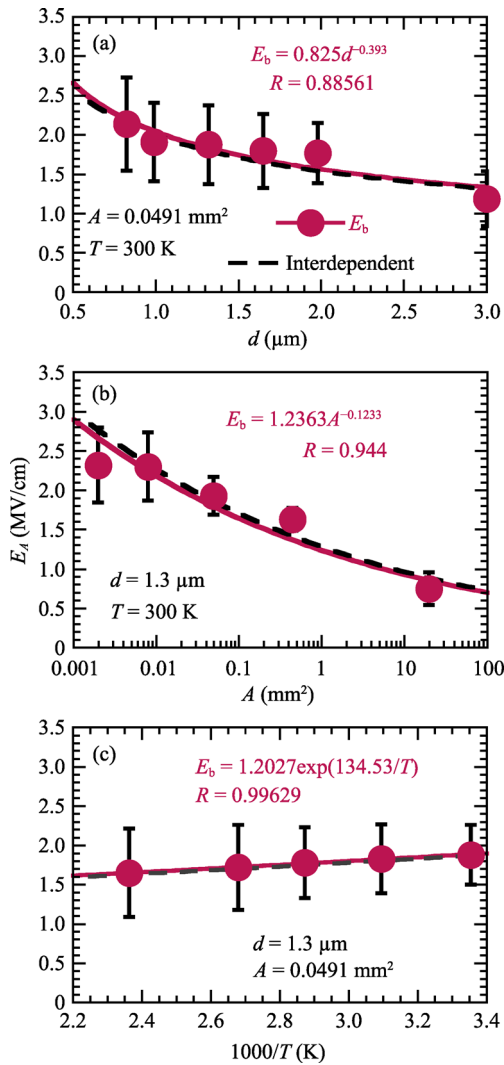
Fig. 3 Average dielectric breakdown electric field (E_A) of PLZT films as function of film thickness (a), electrode area (b), and temperature (c). Solid red curves represent the fits with Eqs. (3) and (6); broken black curves represent the fit using the unified Eq. (7).

exponent α calculated in Fig. 3(a), is ~0.393, which is close to that reported for PZT [6,12].

The dependence of E_A on d, A, and T in Figs. 3(a)–3(c) is fitted with the unified equation (Eq. (7)) including all three variables. The fits are in good agreement with the experimental values. The fitting parameters are: $c = 0.88$ MV/cm, $\alpha = 0.396$, $n = 0.123$, $E_a = 0.238$ eV, and $R = 0.867$. It clearly shows the interdependence of these variables (d, A, and T) which play a vital role in the failure mechanism. Therefore, Eq. (7) can be used in failure analysis by predicting the E_b values. The model can also be used for device optimization in specific applications. For example, the aspect ratio (diameter/thickness) of the thin film is essential to

capacitors for energy storage application. For some energy storage properties such as U_{reco}, the corresponding polarization hysteresis loops were measured with the maximum electric field at E_A.

As shown in Fig. 4, the PLZT films exhibit polarization hysteresis loops with low coercive electric field (E_c) and high saturation polarization (P_s), typical of the relaxors which are prime candidates for energy storage applications [25,26]. Based on Eq. (1), high U_{reco} is expected for materials with large E_b, for a given permittivity. U_{reco} is calculated by integrating the area of the P–E loop. The integrated recoverable energy density of the PLZT films as a function of d, A, and T are plotted in Fig. 5.

Similar to E_b, U_{reco} is also found to be strongly dependent on area and less so on temperature. Greater U_{reco} is observed for samples with higher E_b as shown
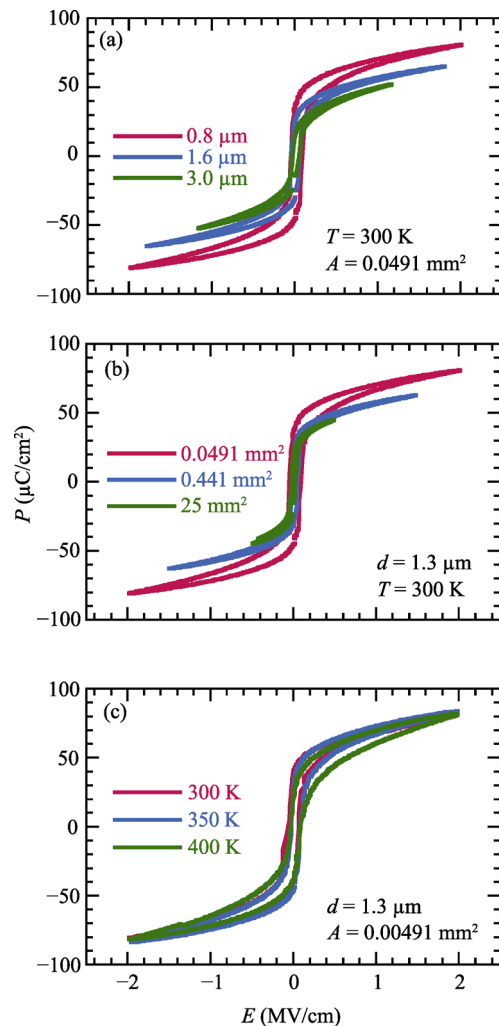
Fig. 4 Polarization hysteresis loops ($E_{max} = E_A$) of PLZT films as a function of film thickness (a), electrode area (b), and measurement temperature (c).
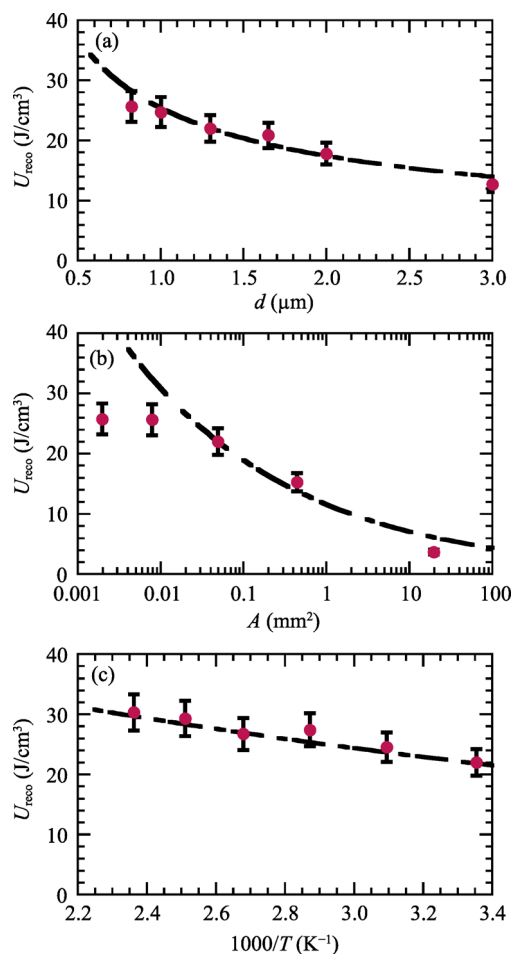
Fig. 5 Recoverable electric energy density (U_{reco}) of PLZT films as function of film thickness (a), electrode area (b), and temperature (c).

in Fig. 5. For example, the value of U_{reco} of the 0.8-μm-thick sample is as high as ~26 J/cm^3 compared to 13 J/cm^3 for the 3-μm-thick film. Similar trend is observed with increasing area, as the E_b decreases with increasing d and A. Based on Eq. (1), we can write $E_{reco} = cd^{-\alpha}A^{-n}\exp(E_a/2kT)$ and fit the data in Fig. 5. The fit (broken lines) is shown in Figs. 5(a)–5(c) and the parameters calculated are: c = 67.5 J/cm^3, α = 0.544, n = 0.213, E_a = 0.534 eV, and R = 0.768. These fitting parameters of α, n, E_a are approximately twice of those obtained in Fig. 3, indicating that U_{reco} is proportional to the square of E_A. This implies that the polarization linearly increases as a function of the applied electric field at fields much greater than E_c. This square relationship agrees well with the fact that the PLZT is characteristically relaxor with nearly reversible P–E loops ($E_c \approx 0.02$ MV/cm).

Currently, the ferroelectric energy densities are typically reported with stressing their thicknesses rather than electrode areas. Given the equation above, it must be pointed out that a reduced electrode area, which is widely adopted in measuring ferroelectric thin films, could also play a role in its higher energy density than that of thicker films.

In conclusion, a unified equation has been developed on the relationship between the E_b and related parameters such as the film thickness, electrode area, and temperature. The model has been found to agree well with the experimental results of the PLZT thin films in terms of all variables. Theoretical fits to the experimental data indicate the interdependence of the processing parameters. Polarization hysteresis loops of PLZT films are also obtained for predicting U_{reco} based on the developed model. A unique relationship of $U_{reco} \propto E_A^2$ is found, that is particularly useful in predicting the electric energy density in terms of variables d, A, and T.

References

[1] Scott JF, Paz de Araujo CA. Ferroelectric memories. *Science* 1989, **246**: 1400–1405.

[2] Setter N, Damjanovic D, Eng L, *et al*. Ferroelectric thin films: Review of materials, properties, and applications. *J Appl Phys* 2006, **100**: 051606.

[3] Gregg JM. Ferroelectrics at the nanoscale. *phys stat sol (a)* 2009, **206**: 577–587.

[4] Tong S. Dielectric and ferroelectric properties of lead lanthanum zirconate titanate thin films for capacitive energy storage. Ph.D. Thesis. Cincinnati (USA): University of Cincinnati, 2012.

[5] Scott JF. High-dielectric constant thin films for dynamic random access memories (DRAM). *Annu Rev Mater Sci* 1998, **28**: 79–100.

[6] Scott JF, Melnick BM, McMillan LD, *et al*. Dielectric breakdown in high-ε films for ULSI DRAMs. *Integr Ferroelectr* 1993, **3**: 225–243.

[7] Lee BH, Kang CY, Choi R, *et al*. Stress field analysis to understand the breakdown characteristics of stacked high-k dielectrics. *Appl Phys Lett* 2009, **94**: 162904.

[8] Li X, Tung CH, Pey KL. The nature of dielectric breakdown. *Appl Phys Lett* 2008, **93**: 072903.

[9] Agarwal VK, Srivastava VK. Thickness dependence of breakdown field in thin films. *Thin Solid Films* 1971, **8**: 377–381.

[10] Chen G, Zhao JW, Li ST, *et al*. Origin of thickness dependent dc electrical breakdown in dielectrics. *Appl Phys Lett* 2012, **100**: 222904.

[11] Forlani F, Minnaja N. Thickness influence in breakdown phenomena of thin dielectric films. *phys stat sol (b)* 1964, **4**: 311–324.

[12] Gerson R, Marshall TC. Dielectric breakdown of porous ceramics. *J Appl Phys* 1959, **30**: 1650–1653.

[13] Lysne PC. Prediction of dielectric breakdown in shock–loaded ferroelectric ceramics. *J Appl Phys* 1975, **46**: 230–232.

[14] Ma BH, Narayanan M, Balachandran U. Development of PLZT film-on-foil capacitors with high dielectric strength. *MRS Proc* 2009, **1199**: 1199-F03-01.

[15] Milliken AD, Bell AJ, Scott JF. Dependence of breakdown field on dielectric (interelectrode) thickness in base-metal electroded multilayer capacitors. *Appl Phys Lett* 2007, **90**: 112910.

[16] Scott JF, Azuma M, Paz de Araujo CA, *et al.* Dielectric breakdown in high-ε films for ULSI DRAMs: II. Barium-strontium titanate ceramics. *Integr Ferroelectr* 1994, **4**: 61–84.

[17] Yoshimura M, Bowen HK. Electrical breakdown strength of alumina at high temperatures. *J Am Ceram Soc* 1981, **64**: 404–410.

[18] O'Dwyer J. Breakdown in solid dielectrics. *IEEE Trans Elect Insul* 1982, **EI-17**: 484–487.

[19] Moon PH. The theory of thermal breakdown of solid dielectrics. *Trans Am Inst Electr Eng* 1931, **50**: 1008–1021.

[20] Dissado L, Fothergill J, Wolfe S, *et al.* Weibull statistics in dielectric breakdown; theoretical basis, applications and implications. *IEEE Trans Elect Insul* 1984, **EI-19**: 227–233.

[21] Sune J. New physics-based analytic approach to the thin-oxide breakdown statistics. *IEEE Electron Device Lett* 2001, **22**: 296–298.

[22] Kimura M. Oxide breakdown mechanism and quantum physical chemistry for time-dependent dielectric breakdown. In: Proceedings of the 1997 IEEE International Reliability Physics Symposium, 1997: 190–200.

[23] Mudholkar GS, Kollia GD. Generalized Weibull family: A structural analysis. *Commun Stat-Theory Methods* 1994, **23**: 1149–1171.

[24] Dissado LA. Theoretical basis for the statistics of dielectric breakdown. *J Phys D: Appl Phys* 1990, **23**: 1582–1591.

[25] Cross LE. Relaxor ferroelectrics. In: *Piezoelectricity*. Heywang W, Lubitz K, Wersing W, Eds. Springer Berlin Heidelberg, 2008: 131–155.

[26] Yamashita Y, Harada K, Saitoh S. Recent applications of relaxor materials. *Ferroelectrics* 1998, **219**: 29–36.